ELSEVIER

Synthetic Metals 139 (2003) 191–200

SYNTHETIC METALS

www.elsevier.com/locate/synmet

Effect of dopants on electron localization length in polyaniline

P.K. Kahol [a,*], K.K. Satheesh Kumar [b], S. Geetha [b], D.C. Trivedi [b]

[a] *Department of Physics, Wichita State University, Wichita, KS 67260-0032, USA*
[b] *Electrochemical Materials Science Division, Center for Studies in Conducting Polymers, Central Electrochemical Research Institute, Karaikudi 630006, India*

Received 12 August 2002; received in revised form 12 November 2002; accepted 12 December 2002

Abstract

The electronic behavior of chemically synthesized polyaniline depends on the amount of disorder—whether homogeneous or inhomogeneous—created during synthesis and doping. Its physical properties are significantly affected by a number of parameters such as catalyst type, solution pH, oxidant/monomer ratio, solvent type, secondary doping, dopant type, dopant size and synthesis temperature. With the view of studying the dependence of electron localization behavior on the dopant type, all other factors remaining the same, we report in this paper a systematic study of NMR, EPR, magnetic susceptibility, and dc conductivity measurements for seven doping acids. The EPR lineshape in all these cases is close to a Lorentzian, but the linewidth is sensitively dependent on the type of the dopant. In spite of differences in the magnitude and the temperature dependences of dc conductivity and magnetic susceptibility data, the experiments reveal a localization length of approximately 30 Å for *all* the samples. It is concluded that, unlike drastically different charge transport behaviors caused by the presence of substituent groups on phenyl rings of the polymer chains, dopant molecules belonging to a given family have virtually no effect on the electron localization length.

Keywords: Polyaniline; Conductivity; Electron paramagnetic resonance; Localization length; Magnetic susceptibility

1. Introduction

The objective of this paper is to investigate the electron localization behavior of polyaniline (PAN) as a function of the dopant type for the following reasons.

First, polyaniline in the emeraldine base form is rendered chemically conductive through doping by exposure to protonic acids [1–7]. The doping or protonation occurs from a general reaction of polyaniline with protonic acids that is of the form H^+M^-, where M^- is the counterion. Although counterions are not a part of the polymer backbone along which charge delocalizes, the presence of suitable counterions has been found to facilitate charge transport. For example, chloride ions through their solvation effect with absorbed water have been implicated in leading to increased conductivity [8]. In addition, the role of structural order in yielding better conducting samples has been amply reported [9,10]. The dc conductivity and structural properties have been shown to vary rather dramatically depending on the molecular weight of the polymer, the nature of the solvent, and the processing conditions to make free-standing films [9]. Such studies have been done primarily on D,L-camphorsulfonic acid (CSA) doped polyaniline and PF_6 doped polypyrrole (PPY), which happen to be the most investigated materials in the area of conducting polymers [10]. The effect on electron localization length due to different dopants belonging to the same family, *with other factors remaining the same*, has not been investigated in detail.

Second, it is now well established that polyaniline when doped with protonic acids can be dissolved in a number of commonly used organic solvents. The dc conductivity of trichlorobenzene-sulfonic acid doped pressed pellet was found to be 10 S/cm, but it turned out to be seven orders of magnitude smaller when films of the same material were cast in the solvent *m*-cresol and three orders of magnitude smaller for films cast in dimethylsulfoxide (DMSO). This result is in sharp contrast to the data on CSA doped polyaniline pellets and films [11,12]. CSA-PANI pellets typically yield a dc conductivity of 50 S/cm, but lead to higher conductivity of the order of 300 S/cm for films cast in *m*-cresol. As an other example of the role of a dopant in affecting the electronic behavior of conducting polyaniline, the dc conductivity of 2-hydroxy-4-methoxy-benzophenone-5-sulfonic acid doped pressed pellet has a value of the order of 10^{-1} S/cm, stays

* Corresponding author. Tel.: +1-316-978-5224; fax: +1-316-978-3350.
E-mail address: pawan.kahol@wichita.edu (P.K. Kahol).

0379-6779/$ – see front matter © 2003 Published by Elsevier Science B.V.
doi:10.1016/S0379-6779(02)01321-8

nearly the same for films cast in *m*-cresol, but it decreases by six orders of magnitude for films cast in DMSO [11,12]. Although both the dopant and solvent play a significant role in the process of charge conduction, transport, magnetic and EPR measurements have not been made to separately investigate these effects quantitatively.

Third, in the inhomogeneous model as it is applied to partially crystalline conducting polymers, the electron localization length (α^{-1}) in the more disordered regions is smaller than the crystalline coherence length (ξ) [13]. The crystalline regions are separated by disordered regions, which lead to increased electron localization with increased disorder. When the polymer chains have a coil-like morphology in the disordered regions, not only is the localization length small for electrons in the disordered regions but the free electrons are also confined within the ordered or metallic regions. Structural disorder is a primary source of localization, and the electron localization length is an indicator of the average amount of disorder in the sample. A determination of α^{-1} in polyaniline that is doped with many different, but closely related, dopants can provide insights into the effect of the nature of a dopant on the electronic behavior of conducting polymers.

Fourth, the presence of substituent groups on the benzene rings has been shown to have a considerable effect on the electronic properties of polymers. Poly(*o*-toluidine) (POT), for example, exhibits reduced interchain bandwidth and interchain coherence [14,15]. Compared to PANI, these effects in POT are due to the steric size of the CH_3 groups and the increased disorder due to the random placement of CH_3 groups on ring sites, respectively. The electron localization in POT is five times smaller compared with the value in PANI. However, the disorder in POT fibers, drawn from a solution of POT powder with a suitable solvent, is lower and consequently the localization length is higher. As an other example, the electron localization length was found to be much larger in poly(alkoxyanilines) compared with their respective poly(alkylanilines) [16]. The larger localization length in poly(alkoxyaniline) compared with poly(alkylaniline) seems to arise from reduced Coulomb interaction between the positive charge on the polymer chain and the anion due to the electron donating nature of the alkoxy groups. The purpose of this paper is to investigate the effect of the presence of dopant molecules of the same family on the electron localization behavior of polyaniline (when the size of the dopant is not changed significantly).

Fifth, a dc conductivity study on polyaniline films cast in chloroform, benzyl alcohol (BeOH) and *m*-resol, but doped with benzene sulfonic acid (BSA), *para*-toluenesulfonic acid (PTSA), camphor sulfonic acid (CSA) and naphthalene sulfonic acid (NSA), has been reported [17]. Since the dc conductivity behaves like $\exp[-(T_0/T)^{1/2}]$ and $T_0 = 16/[k_B N(E_F)\alpha^{-1}]$, the authors have determined a localization length (α^{-1}) from the temperature dependence of the dc conductivity. It is reported that the localization lengths in *m*-cresol cast films of polyaniline are 80, 51, 38, 25 Å for the dopants BSA, CSA, PTSA and NSA, respectively. For films cast in chloroform, the localization lengths are 34, 32, 29 and 27 Å for the dopants BSA, CSA, PTSA and NSA, respectively. For the third solvent BeOH, the localization lengths are 25, 25, 28 and 49 Å for the dopants BSA, CSA, PTSA and NSA, respectively. Although we do not know how, without the knowledge of $N(E_F)$, α^{-1} can be obtained from T_0, a few observations are in order from their measurements and analysis. First, α^{-1} exhibits a large range of values for the four dopants in the solvent *m*-cresol. Second, α^{-1} in the BeOH cast films does not change for the dopants BSA, TSA and CSA, but surprisingly shows an increase by a factor of two in the case of the dopant NSA. Third, the four dopants in the case of chloroform cast films also do not show any significant change in α^{-1}. Before determining the role of secondary doping on the electronic properties such as the localization length, it is rather important to know the magnitudes of the localization length before introducing secondary processing of chain morphology in the polymer.

Sixth, some differences were observed in our earlier magnetic, optical, and EPR studies of polyaniline that was doped with *para*-toluenesulfonic acid (PTSA) and sulfosalicylic acid (SSA) [18]. We decided to investigate the electronic behavior of polyaniline doped with a number of dopants belonging to the same family.

In general, polyaniline is among the most studied conducting polymers due to its relatively high conductivity, environmental stability, ease of preparation and low cost of raw materials. Fundamental interest in polyaniline stems from the possibility of investigating physics in different states, such as the “Fermi glass” state [19], the “granular metal” state [13,20,21], or as a “disordered metal” close to the metal–insulator transition state [9]. Polyaniline’s technological significance arises due to its processability into films and fibers [22], which is achieved by synthesizing soluble conducting polyaniline either by using functionalized protonic acids, such as *para*-toluene sulfonic acid [23], benzene sulfonic acid [23], sulfanilic acid [24], sulfamic acid [25], camphorsulfonic acid [20], dodecyl-benzene sulfonic acid [20], octyl-benzene sulfonic acid [26], sulfosalicylic acid [27] or methane sulfonic acid [28] as dopants, or by including substituent groups in the ring giving polymers such as alkyl polyanilines [29], alkoxy polyanilines [30], sulfonic acid ring-substituted polyanilines (SPAN) [31], and highly sulfonated SPAN [32]. The quality of the synthesized material undoubtedly depends on the combination of mesoscopic homogeneous order and microscopic disorder created during the synthesis and doping processes. These factors significantly affect localization of the electron wave function [21,22,33].

Seven dopants have been chosen for the present study, and their chemical names and abbreviations are: (1) 2,5-dimethylbenzenesulfonic acid (PXSA), (2) 3,4-dimethylbenzenesulfonic acid (OXSA), (3) 4-hydroxybenzenesulfonic acid (PSA), (4) 4-hydroxy-*m*-benzenedisulfonic acid (PDSA), (5) 4,6-dihydroxy-*m*-benzenedisulfonic acid (RDSA), (6)

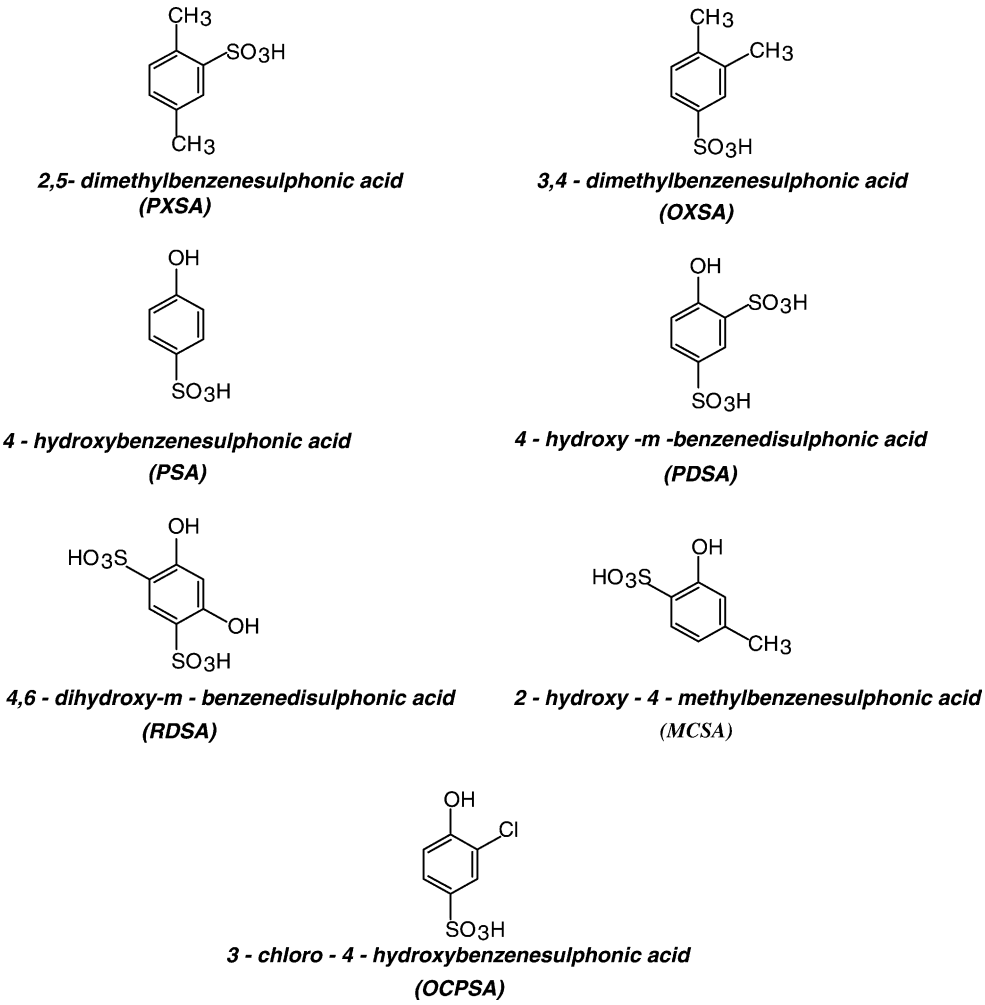

Fig. 1. Structural and chemical formulas, and their abbreviated names for the seven dopants used in the present study.

2-hydroxy-4-methylbenzenesulfonic acid (MCSA), and (7) 3-chloro-4-hydroxybenzenesulfonic acid (OCPSA). The chemical structure of these dopants is also shown in Fig. 1. The size is not too drastically changed from one dopant to the other in this series.

2. Experimental

2.1. Sample synthesis

2.1.1. Synthesis of polyaniline

Ammonium peroxy disulphate (0.1 M aqueous solution in HCl) was added dropwise to a stirred solution of 0.1 M aniline dissolved in 1 M aqueous solution of HCl, that was pre-cooled to a temperature in the range 0–5 °C. Ammonium peroxy disulphate was added very slowly to prevent warming of the solution. After completion of the addition (addition time almost 4–6 h), stirring was continued for 2 h to ensure completion of the reaction. At the end of the reaction acetone was added to terminate the polymerization reaction and the mixture was filtered under suction. Collected green precipitates of emeraldine hydrochloride were washed repeatedly with distilled water till these washings were colorless. The filtered and washed precipitates were then treated with aqueous solution of ammonia (pH $\approx$ 9) under stirring for 6–8 h for effective undoping to obtain emeraldine base. This reaction mixture was filtered, washed with distilled water till washings were neutral to a pH indicator paper.

The blue emeraldine base powder, obtained after filtration, was purified by refluxing with methyl alcohol, benzene and acetone. This process of treatment with organic solvents was repeatedly done till the filtrate was colorless. Finally, the blue emeraldine base obtained was dried under dynamic vacuum at 60–80 °C for 8 h.

The fine powder of blue emeraldine base thus obtained was dispersed in 1 M aqueous solution of functionalized aromatic sufonic acids like 2,5-dimethylbenzenesulfonic acid, 3,4-dimethylbenzenesulfonic acid, 4-hydroxybenzenesulfonic acid, 4-hydroxy-*m*-benzenedisulfonic acid, 4,6–dihydroxy-*m*-benzenedisulfonic acid, 2-hydroxy-4-methylbenzene sulfonic acid and 3-chloro-4-hydroxybenzenesulfonic acid

under vigorous stirring for 24 h. After doping reaction, solution was filtered under suction and collected material was given washing with 1 M aqueous solution of functionalized aromatic sulfonic acid. By this method, a doping level of 50 mol% was achieved. The so obtained polymer was dried at 60–80 °C under dynamic vacuum for 12 h [34].

As synthesized doped polyaniline samples were found to have a moisture content as follows: PXSA 2%, OXSA 2.5%, PSA 3.75%, PDSA 3.5%, RDSA 5%, MCSA 2% and OCPSA 5%. Complete degradation of the polymers occurs around 607–685 °C.

The acids used in this study were synthesized and purified according to standard synthetic organic chemistry methodologies [35–41], as described in the following sections.

2.1.2. 2,5-Dimethylbenzenesulfonic acid

Place 5.2 g (6 ml, 0.05 M) of *p*-xylene in a 25 ml round bottomed flask and add, with gentle swirling agitation, 10 ml of concentrated sulfuric acid. Heat the mixture on water bath for 10–15 min, remove the flask from the bath and mix the contents with a circular motion every 2 min. The reaction is complete when the xylene layer on the surface of the acid has disappeared. Cool the mixture to room temperature and add 5 ml of H_2O cautiously with gentle swirling. Pour the warm reaction mixture into a 100 ml beaker and cool in ice. Filter the crystalline solid with suction on a sintered glass funnel. Recrystallize the crude product from 5 ml of water and dry on filter paper. The yield of 2,5-dimethylbenzenesulfonic acid is 90% and its melting point is 82 °C [35].

2.1.3. 3,4-Dimethylbenzenesulfonic acid

A volume of 25 ml (22 g) of technical *o*-xylene (95%, with boiling point at 143–144 °C) and 12.5 ml of concentrated sulfuric acid were stirred together at 95 °C for 10–15 min. When the mixture was cooled a small layer of unsulphonated material was separated. The sulfonic acid layer diluted with 15 ml of water was then neutralized with 40% NaOH solution. The solid, which separated on cooling, was collected on a centrifuge and recrystallized from half its weight of distilled water. The sodium salt obtained is then converted into its free acid form by *Amberlite IRP-69* resin. The melting point of this acid was found to be 63–64 °C [36].

2.1.4. 4-Hydroxybenzenesulfonic acid

Place 9.5 g (0.1 mol) of phenol in a dry 500 ml flat-bottomed flask and add 23 g (12.5 ml) of concentrated sulfuric acid. Shake the mixture (which becomes warm) and heat it on a boiling water bath for 30 min to complete the formation of the *o*- and *p*-phenolsulfonic acids (2:3). Then cool the flask thoroughly in an ice–water mixture. The *o*- and *p*-phenolsulfonic acid can be separated by means of barium and magnesium salts [37].

2.1.5. 4-Hydroxy-m-benzenedisulfonic acid

Place a mixture of 31 g (0.33 M) of phenol in a dry 500 ml flat-bottomed flask and add 116 g of concentrated sulfuric acid. Heat in a boiling water bath for 3 h with mechanical stirring. On cooling to room temperature or below by immersing the flask in ice water and then adding slowly a solution of 95 g of NaOH in 235 ml water, solid salt separates. Due to its hygroscopic nature, melting point could not be measured [38].

2.1.6. 4,6-Dihydroxy-m-benzenedisulfonic acid

Carefully add 25 ml of concentrated sulfuric acid (98%) to 5.5 g of (0.05 M) of resorcinol in a 150 ml beaker whilst stirring the mixture continuously with the glass rod. Then warm the mixture to 60–65 °C on a water bath and allow it to stand for 15 min. Cool the slum of the 4,6-disulfonic acid to 0–10 °C, which is then converted into sodium salt by adding NaOH [39].

2.1.7. 2-Hydroxy-4-methylbenzenesulfonic acid

An volume of 10 ml of *m*-cresol and 10 ml of concentrated sulfonic acid were mixed and refluxed for 1 h at 120 °C. Cooled the reaction mixture to room temperature, then converted to sodium salt by adding NaOH. Due to its hygroscopic nature, melting point could not be measured [40].

2.1.8. 3-Chloro-4-hydroxybenzenesulfonic acid

An amount of 12.6 g of *o*-chlorophenol and 10 ml of concentrated sulfuric acid were stirred together on a water bath for about 30 min. Cooled the mixture to 0 °C, which is then converted into the sodium salt by adding NaOH. Due to its hygroscopic nature, melting point could not be measured [41].

2.2. NMR measurements

The NMR measurements were made on a Varian Inova 400 MHz spectrometer. Samples were dissolved in deuterated DMSO-d6 (Cambridge Isotope Ltd.) and were left overnight before recording the spectra.

2.3. Electrical dc conductivity, $\sigma(T)$

Powders pressed into round pellets of thickness ~0.05 cm were used for conductivity measurements. Samples cut into the shape of a parallelepiped were mounted on the cold finger of a Janis closed cycle refrigerator. Conductivity was measured on both the pressed pellets and the thin films by the four-probe technique. Acheson Electrodag 502 was used to make contact between the copper wire and the pellet. Temperature was controlled with a Lake Shore temperature controller and the absolute temperature was measured using a calibrated Lake shore temperature sensor. A Keithley Model No. 220 constant current source was used to pass a constant current through the sample and the voltage was measured using a Keithley Model No. 614 Electrometer. The $\sigma(T)$ was measured in the Ohmic region from room temperature down to about 30 K.

2.4. Electron spin resonance

A small quantity of powdered sample was placed in an EPR tube for ESR studies. A computer-controlled X-band Bruker EMX 6/1 spectrometer was used for the ESR experiments. Microwave power and magnetic field modulation were carefully optimized to avoid any lineshape distortion. The modulation amplitude was kept in the range 0.1–0.5 G. Variable temperature measurements down to about 10 K were made using a Bruker digital temperature controller (ER4112HV and ER4121VT).

3. Results and discussion

3.1. Structural studies using ^1H NMR

Fig. 2 shows the room temperature NMR spectra of four representative samples namely, OCPSA-PANI, PDSA-PANI, PSA-PANI and RDSA-PANI. The NMR assignments are relative to TMS as a standard. Theoretical chemical shift calculations for all the seven dopants were done using CS Chemdraw Ultra program (version 4.0, Cambridgesoft Corp.) and these are shown in Fig. 3. We do find a fairly close match between the theoretical and observed chemical shift values, and the downfield or upfield peak shifts arise due to the nature of the solvent. It is clear that dopants are released into DMSO from the polymer. Low-intensity peaks in the aromatic region are believed to be due to the partially dissolved polymer in DMSO. In summary, the NMR analysis provides evidence in support of the integrity of the seven dopants.

3.2. EPR linewidth

The EPR peak-to-peak linewidth (Δ_{pp}) as a function of temperature is shown in Fig. 4. The samples were pumped overnight under a vacuum of about 1×10^{-4} Torr to remove

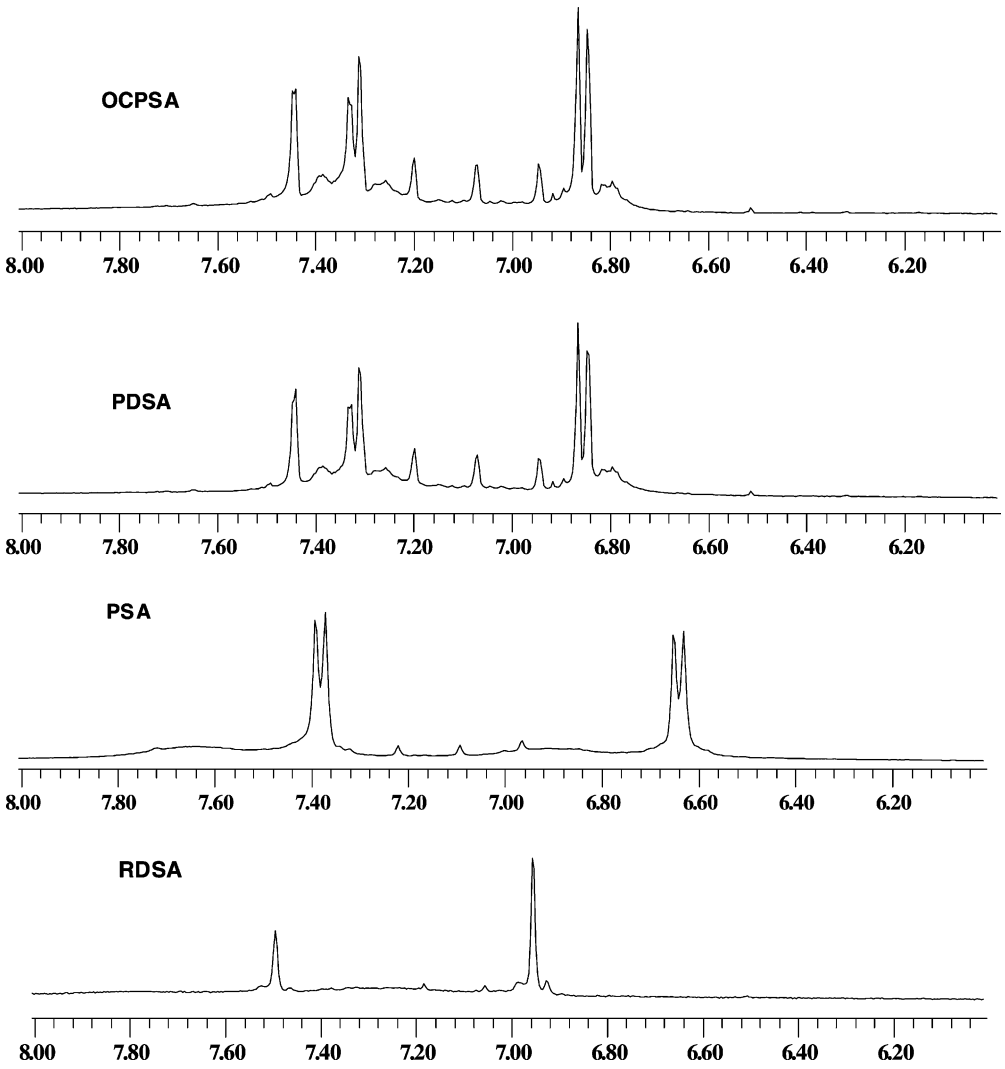

Fig. 2. Experimental proton NMR spectra of polyaniline doped with the four dopants namely, RDSA, PSA, PDSA and OCPSA.

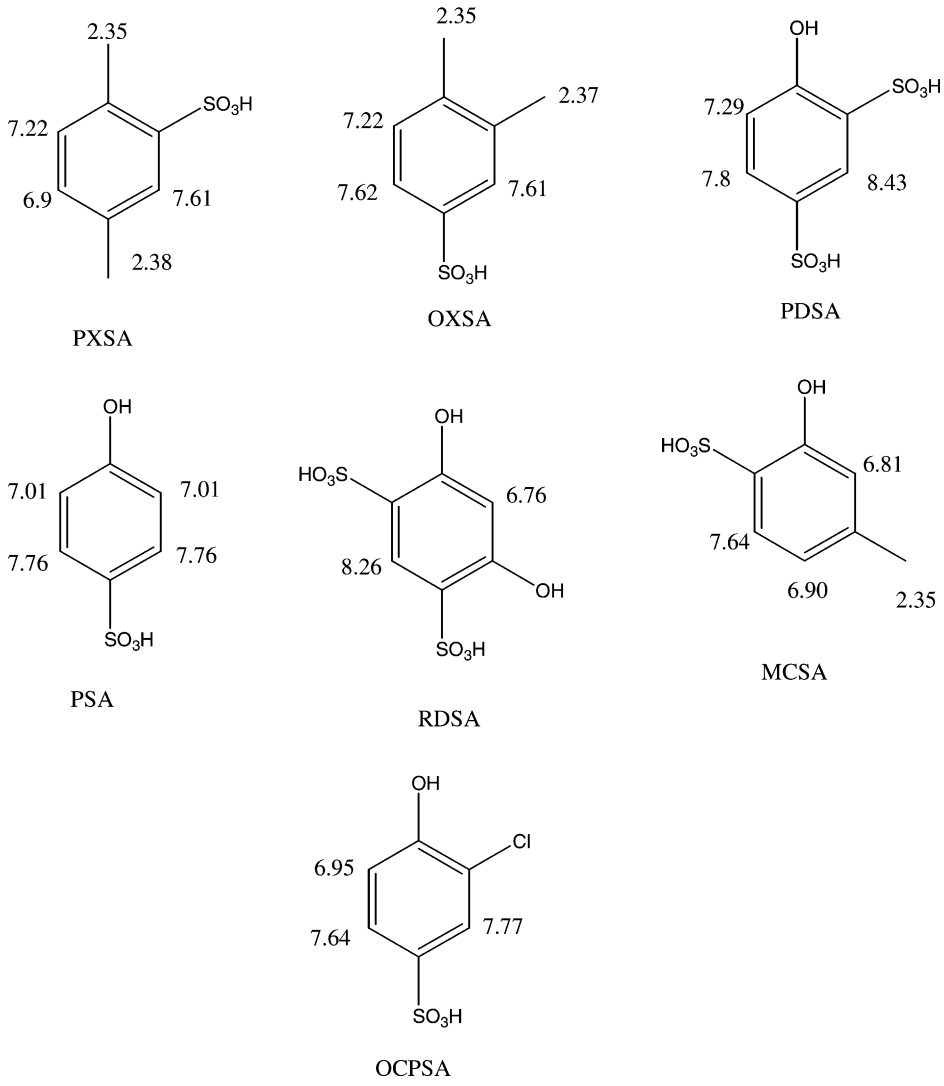

Fig. 3. Theoretical values of the proton chemical shift values indicated on the respective proton sites.

oxygen and moisture. At temperatures higher than 100 K or so, Δ_{pp} is found to be proportional to temperature. At low temperatures, however, Δ_{pp} increases with decrease in temperature. The minimum around 100 K is found for all the samples except OCPSA-PANI and is rather very broad. In the case of OCPSA-PANI, Δ_{pp} increases very slowly with decrease in temperature down to 100 K.

The EPR linewidth that shows a linear dependence on temperature at higher temperatures is essentially determined by the spin–lattice relaxation time, which is proportional to temperature for direct process involving absorption of single phonons. Spin localization is the reason for an increase of Δ_{pp} with decrease in temperature at lower temperatures. It is worth recalling that the EPR linewidth behavior was qualitatively the same as observed here for polyaniline samples protonated with HCl [14].

One of the most obvious features of Fig. 4 is the result that the data for the peak-to-peak linewidth, including the temperature dependence, falls into three distinct categories. The room-temperature linewidth is around 5.8 G in the case of PSA-PANI, PDSA-PANI and RDSA-PANI (samples 3, 4 and 5), around 3 G in the case of PXSA-PANI, OXSA-PANI and MCSA-PANI (samples 1, 2 and 6), and 1.3 G in the case of OCPSA-PANI (sample 7). While the dopants in samples 3, 4 and 5 have only OH and SO_3H (single or double) substituent groups and give rise to the top set of linewidth curves, the dopants in samples 1 and 2 contain two CH_3 units and a SO_3H unit and yield the middle set of curves. Since the dopant in sample 6 contains one OH group in addition to CH_3 and SO_3H groups, the magnitude of Δ_{pp} is larger than that for samples 1 and 2 at all temperatures. Finally, for the dopant OCPSA that contains the substituent Cl in addition to OH and SO_3H, Δ_{pp} is the lowest and it increases very slowly with a decrease in temperature. It is therefore abundantly clear that the EPR linewidth is very sensitively dependent on the dopant type.

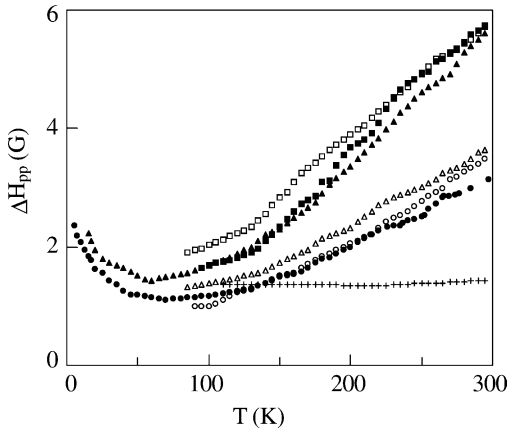

Fig. 4. Dependence of the peak-to-peak EPR linewidth (Δ_{pp}) as a function of temperature: PXSA-PANI (solid circles); OXSA-PANI (open circles); PSA-PANI (solid squares); PDSA-PANI (open squares); RDSA-PANI (solid triangles); MCSA-PANI (open triangles); OCPSA-PANI (plusses).

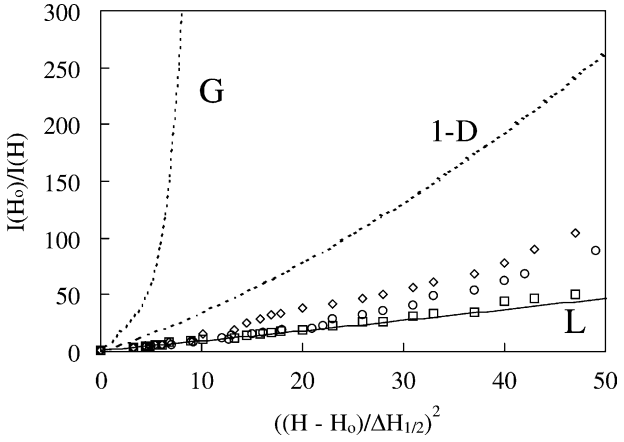

Fig. 5. The lineshape results on: OXSA-PANI (open circles); RDSA-PANI (open squares); OCPSA-PANI (open diamonds). The theoretical lineshapes corresponding to a Lorentzian function (continuous line), a Gaussian function (dashed line), and a function indicating one-dimensional spin motion (dashed-dot line) are also shown in this plot.

3.3. EPR lineshape

Fig. 5 shows the EPR absorption lineshape at 110 K for the three samples: PSA-PANI, RDSA-PANI, and OCPSA-PANI. The *x*-axis in this plot is the square of the magnetic field from the central value after dividing this difference by the full width at half-maximum ($\Delta H_{1/2}$). The *y*-axis, on the other hand, is the ratio of the intensity at the central magnetic field (H_0) and the intensity at a given field *H*. The lineshape in all these cases is close to a Lorentzian for a magnetic field approximately six times the $\Delta H_{1/2}$.

3.4. EPR magnetic susceptibility

Fig. 6 shows results for the EPR magnetic susceptibility, plotted as χT versus *T*, for the seven samples. The measurements for PXSA-PANI and RDSA-PANI were also

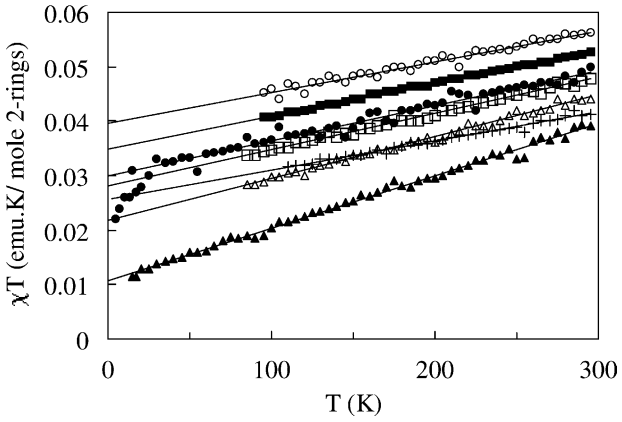

Fig. 6. Dependence of the magnetic susceptibility as a function of temperature, plotted as χT vs. *T*, for the seven samples: PXSA-PANI (solid circles); OXSA-PANI (open circles); PSA-PANI (solid squares); PDSA-PANI (open squares); RDSA-PANI (solid triangles); MCSA-PANI (open triangles); OCPSA-PANI (plusses). The solid lines are fits of the linear part of the data to Eq. (1).

extended to temperatures below 77 K. The data can be fitted to an Equation of the type $\chi = \chi_P + C/T$, which summarizes the fact that the measured susceptibility is a sum of temperature-independent Pauli and temperature dependent Curie susceptibilities. The Pauli and Curie susceptibilities can be obtained from the linear part of the χT versus *T* plot because

$$\chi T = \chi_P T + C, \tag{1}$$

where *C* is the Curie constant. Fig. 6, thus, also shows fits of the data to Eq. (1) in the form of continuous lines. The slope of the χT versus *T* plots yields χ_P, which can be used to obtain $N(E_F)$ using $\chi_P = [\mu_B^2 N(E_F)]$. The knowledge of $N(E_F)$ and T_0 will yield values for the localization length, α^{-1}. The constant *C* is related to the number of Curie spins (n_C) in the sample.

The values of χ_P, arising from fits of the data, for the samples 1 through 7 are, respectively, 65×10^{-6}, 55×10^{-6}, 60×10^{-6}, 67×10^{-6}, 95×10^{-6}, 75×10^{-6}, and 70×10^{-6} emu/(mol 2-rings). The respective values of *C* for the seven samples are: 0.030, 0.039, 0.035, 0.028, 0.011, 0.022, and 0.026 emu K/(mol 2-rings).

3.5. The dc conductivity

As far as dc electrical conductivity is concerned, all the seven samples are found to obey the relation

$$\sigma = \sigma_0 \exp\left(-\frac{T_0}{T}\right)^{1/2} \tag{2}$$

which is characteristic of quasi-one-dimensional variable range hopping between nearest neighbors [14,15,42]. Here,

$$T_0 = \frac{16}{[\alpha^{-1} N(E_F) z k_B]} \tag{3}$$

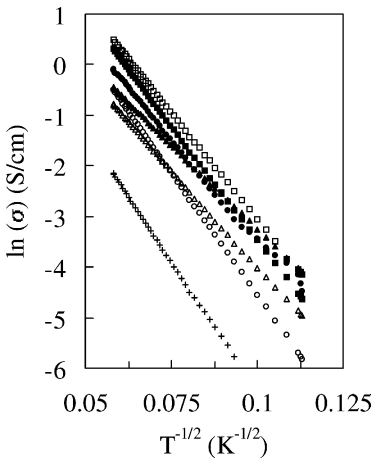

Fig. 7. Dependence of dc conductivity on temperature, plotted as $\ln\sigma$ vs. $T^{-1/2}$, for the seven samples: PXSA-PANI (solid circles); OXSA-PANI (open circles); PSA-PANI (solid squares); PDSA-PANI (open squares); RDSA-PANI (solid triangles); MCSA-PANI (open triangles); OCPSA-PANI (plusses).

$$\sigma_0 = e^2 N(E_F) b^2 \nu_{phonon} \frac{2\pi t_0 \tau_i / h^2}{A} \quad (4)$$

where α^{-1} is the decay length of the localized electron state, $N(E_F)$ the density of states at the Fermi level, z the number of nearest neighbor chains (which is 4 for polyaniline [36]), k_B the Boltzmann constant, b the interchain separation, t_0 the transfer integral, τ_i the mean free time and A is the average cross-sectional area of a chain. A fit of the experimental data to Eq. (2) gives T_0. The determination of $N(E_F)$ from magnetic susceptibility measurements was discussed in the previous section. α^{-1} can therefore be determined by using values of T_0 and $N(E_F)$.

Fig. 7 shows the results of dc conductivity $\sigma(T)$, plotted as $\log\sigma$ versus $T^{-1/2}$, on pressed pellets of the seven samples. It is found that σ for all the samples, except OCPSA whose value is 1×10^{-1} S/cm, lies in the range 1.0 ± 0.6 S/cm. The values of T_0 obtained from the above plots are 7200, 9600, 8500, 7400, 4600, 6200, and 11,000 K for the samples 1 through 7, respectively.

Except for OCPSA-PANI, which exhibits the smallest conductivity and the largest T_0 compared to the six other samples, we do not see in our results any correlation between T_0 and the room temperature conductivity.

3.6. Determination of localization length

Table 1 lists the following quantities: σ at room temperature (σ_{RT}), T_0, χ_P, number of Curie spins (n_C), $N(E_F)$, and α^{-1} as determined from Eq. (3). The value of α^{-1} for all the samples, except OCPSA-PANI, is seen to be nearly the same. This is a rather surprising result especially because no significant correlation was observed between σ_{RT} and T_0.

The local structural order in the polyaniline family is a function of various synthesis parameters of a particular chemical procedure [43,44], but the formation of an inhomogeneous structure—comprised of relatively ordered semi-crystalline regions separated by disordered regions—seems like a common occurrence in the polyaniline system. The chains in the amorphous regions show a coil-like morphology and improved synthesis techniques can introduce instead a rod-like chain morphology in these regions. It is therefore the case that the nature of the disordered regions is not significantly affected by the seven dopants considered in this paper. As is known, the CSA dopant leads to higher conductivity in polyaniline films (PANI-CSA) when they are cast in *m*-cresol as a solvent [7,9,10]. The solvent is thought to act as a secondary dopant, which induces rod-like chain geometries in the amorphous regions. Along similar lines, PAN-CSA-fibers, cast using *m*-cresol, are more insulating than PAN-CSA-films [45], suggesting the presence of more disordered regions in fibers; this conclusion is consistent with X-ray structural studies [43]. On the other hand, the fibers of CSA doped poly(*o*-toluidine) in *m*-cresol (POT-CSA-fibers) exhibit a 1000-fold increase in conductivity compared with POT-HCl-pressed pellets, yet the two systems have comparable amount of crystalline order.

While the localization length for all the samples turns out to be nearly the same, the EPR linewidth shows a distinct dependence on the nature of the dopant. This difference is easy to understand because EPR is sensitive to local magnetic interactions, but a calculation of the localization length involves mesoscopic information about the polymer. The localization length depends on the morphology of the disordered regions, and it is larger for the rod-like morphologies compared with the coil-like morphologies. Although most of the charge is stored as localized spinless bipolarons in the disordered regions, conduction between two ordered regions occurs via diffusion along quasi one-dimensional chains,

Table 1
Room temperature conductivity (σ_{RT}), T_0, χ_P, n_C, $N(E_F)$ and α^{-1} for the seven samples of polyaniline

Sample (molecular mass in g)	σ_{RT} (S/cm)	T_0 (K)	χ_P (10^{-6} emu/mol 2-rings)	n_C (per 2-rings)	$N(E_F)$ (states/eV 2-rings)	α^{-1} (Å)
PXSA-PANI (186, with $2H_2O$)	0.9	7225	65	0.088	2.0	32
OXSA-PANI (186, with $2H_2O$)	0.6	9600	55	0.107	1.7	28
PSA-PANI (174)	1.4	8500	60	0.093	1.9	29
PDSA-PANI (254)	1.6	7430	67	0.075	2.1	30
RDSA-PANI (270)	1.0	4900	95	0.027	2.9	32
MCSA-PANI (177)	0.5	6240	75	0.059	2.3	32
OCPSA-PANI (208, with $1H_2O$)	0.1	11000	51	0.069	1.6	27

which connect these ordered regions, running through disordered regions. The fact that α^{-1} ($\approx$30 Å) is nearly the same in polyaniline doped with different dopants is therefore suggestive of the presence of such isolated chains that stay statistically as well as electronically unaffected by disorder. Furthermore, the chain morphology in the disordered regions must also be of the same type with the implication that the disorder due to the presence of coil-like morphologies in the disordered regions dominates the electron localization behavior of polymers.

While the nature of the dopant in the family of doping acids considered in this paper does not affect the localization length, smaller magnitude for the localization length compared with the HCl-doped polyaniline is believed to be due to the larger size of the dopants.

4. Conclusions

On the basis of the results presented in this paper, we have arrived at the following conclusions. First, the EPR peak-to-peak linewidth that arises from motional as well as spin–lattice relaxational effects is sensitively dependent on the type of the dopant in polyaniline doped with organic doping acids. Second, the EPR magnetic susceptibility and dc electrical conductivity measurements on polyaniline doped with various organic acids reveal a localization length that is approximately the same and falls in the range 27–32 Å. The finding of a nearly constant localization length leads us to the conclusion that the charge transport properties are not significantly affected by the nature of the dopants belonging to a given family. The disorder due to the presence of coil-like morphologies in the disordered regions seems to dominate the electron localization behavior of polymers. This set of systems is therefore ideal for investigating dopant–solvent–polymer interactions through a study of the electron localization lengths. Finally, room temperature dc conductivity data must be combined with the temperature dependent conductivity and magnetic susceptibility measurements to obtain a semi-quantitative understanding of the effects of mesoscopic disorder in polyaniline and related materials.

Acknowledgements

PKK acknowledges partial support of this work from the Petroleum Research Fund that is administered by the American Chemical Society under the Grant number: ACS-PRF #36902-B7. KKS and SG thank the Council of Scientific and Industrial Research (CSIR), New Delhi for the Award of Senior Research Fellowship. Finally, DCT thanks the Department of Science and Technology (DST), Government of India, New Delhi for funding a project SP/SI/G33/94.

References

[1] T.A. Skotheim, R.L. Elsenbaumer, J.R. Reynolds (Eds.), Handbook of Conducting Polymers, Marcel Dekker, New York, 1998.
[2] A.J. Epstein, Springer Series in Materials Science, vol. 41, Organic Electronic Materials, 2001, p. 3.
[3] V.N. Prigodin, A.J. Epstein, Synth. Met. 125 (2002) 43.
[4] A.J. Epstein, V.N. Prigodin, Polym. Mater. Sci. Eng. 86 (2002) 2.
[5] B. Dufour, P. Rannou, J.P. Travers, A. Pron, M. Zagorska, G. Korc, I. Kulszewicz-Bajer, S. Quillard, S. Lefrant, Macromolecules 35 (2002) 6112.
[6] D. Djurado, J. Combet, M. Bee, P. Rannou, B. Dufour, A. Pron, J.P. Travers, Phys. Rev. B: Condens. Matter Mater. Phys. 65 (2002) 184202/1.
[7] A. Wolter, P. Rannou, J.P. Travers, B. Gilles, D. Djurado, Phys. Rev. B: Condens. Matter Mater. Phys. 58 (1998) 7637.
[8] P.K. Kahol, H. Guan, B.J. McCormick, Phys. Rev. 44 (1991) 10393.
[9] R. Menon, in: H.S. Nalwa (Ed.), Handbook of Organic Conductive Molecules and Polymers, vol. 4, Wiley, New York, 1997, p. 47.
[10] R.S. Kohlman, A.J. Epstein, in: T.R. Skotheim, R.L. Elsenbaumer, J.R. Reynolds (Eds.), Handbook of Conducting Polymers, Marcel Dekker, New York, 1997, p. 85.
[11] Y. Cao, P. Smith, A.J. Heeger, Synth. Met. 48 (1992) 91.
[12] Y. Cao, J. Qiu, P. Smith, Synth. Met. 69 (1995) 187.
[13] A.G. MacDiarmid, A.J. Epstein, Synth. Met. 65 (1994) 103.
[14] Z.H. Wang, H.H.S. Javadi, A. Ray, A.G. MacDiarmid, A.J. Epstein, Phys. Rev. B 42 (1990) 5411.
[15] (a) N.J. Pinto, P.K. Kahol, B.J. McCormick, N.S. Dalal, H. Wan, Phys. Rev. B 49 (1994) 13983;
(b) P.K. Kahol, N.J. Pinto, B.J. McCormick, Solid State Commun. 91 (1994) 21.
[16] A. Raghunathan, P.K. Kahol, B.J. McCormick, Synth. Met. 100 (1999) 205.
[17] J. Joo, H.G. Song, Y.C. Chung, J.S. Baeck, S.K. Jeong, J.S. Suh, E.J. Oh, J. Korean Phys. Soc. 30 (1997) 230.
[18] A. Raghunathan, T.S. Natarajan, G. Rangarajan, S.K. Dhawan, D.C. Trivedi, Phys. Rev. B 47 (1993) 13189.
[19] F. Wudl, R.O. Angus, F.L. Lu, D.M. Allemand, D.J. Vachon, M. Nowak, Z.X. Liu, A.J. Heeger, J. Am. Chem. Soc. 109 (1987) 3677.
[20] A.J. Epstein, J.M. Ginder, F. Zuo, R.W. Bigelow, H.S. Woo, D.B. Tanner, A.F. Richter, H.S. Huang, A.G. MacDiarmid, Synth. Met. 18 (1987) 303.
[21] A.J. Epstein, A.G. MacDiarmid, Makromol. Chem., Macromol. Symp. 51 (1991) 217.
[22] R. Menon, C.O. Yoon, D. Moses, A.J. Heeger, Y. Cao, Phys. Rev. B 48 (1993) 17685.
[23] S.K. Dhawan, D.C. Trivedi, Polym. Int. 25 (1991) 55.
[24] S. Li, Y. Cao, Z. Xue, Synth. Met. 20 (1987) 141.
[25] S.K. Dhawan, D.C. Trivedi, J. Appl. Electrochem. 22 (1992) 563.
[26] A. Kobayashi, X. Xu, H. Ishikawa, M. Satoh, E. Hasegawa, J. Appl. Phys. 72 (1992) 5702.
[27] D.C. Trivedi, S.K. Dhawan, Synth. Met. 58 (1993) 309.
[28] B. Sanjai, A. Raghunathan, T.S. Natarajan, G. Rangarajan, S. Thomas, P.V. Prabhakaran, S. Venkatachalam, Phys. Rev. B 55 (1997) 10734.
[29] D. Maccines, L.B. Funt, Synth. Met. 25 (1988) 235.
[30] W.A. Gazotti Jr., Marco A. De Paoli, Synth. Met. 80 (1996) 263, and references therein.
[31] J. Yue, Z.H. Wang, K.R. Cromack, A.J. Epstein, A.G. MacDiarmid, J. Am. Chem. Soc. 113 (1991) 2665.
[32] X.-L. Wei, Y.Z. Wang, S.M. Long, C. Bobeczo, A.J. Epstein, J. Am. Chem. Soc. 118 (1996) 2545.
[33] J.-C. Chiang, A.G. MacDiarmid, Synth. Met. 13 (1986) 193.
[34] D.C. Trivedi, in: H.S. Nalwa (Ed.), Handbook of Organic Conductive Molecules and Polymers, vol. 2, Wiley, New York, 1997, pp. 505–572.

[35] Vogel's Textbook of Practical Organic Chemistry, IVth ed., ELBS, UK, 1978, p. 644.
[36] H.T. Clarke, E.R. Taylor, J. Am. Chem. Soc. 45 (1923) 831.
[37] Vogel's Textbook of Practical Organic Chemistry, IVth ed., ELBS, UK, 1978, p. 748.
[38] R. King, J. Chem. Soc. 119 (1921) 2108.
[39] Vogel's Textbook of Practical Organic Chemistry, IVth ed., ELBS, UK, 1978, p. 747.
[40] R.D. Haworth, A. Lapworth, J. Chem. Soc. 125 (1924) 1299.
[41] O. Linder, in: W. Gerhartz (Ed.), Ullmann's Encyclopedia of Industrial Chemistry, vol. A3, VCH Verlagsgesellschaft mbH, Weinheim, 1985, p. 507.
[42] E.P. Nakhmedov, V.N. Progodin, A.N. Samukhin, Sov. Phys. Solid State 31 (1989) 368.
[43] J.P. Pouget, Z. Oblakowski, Y. Nogami, P.A. Albouy, M. Laridjani, E.J. Oh, Y. Min, A.G. MacDiarmid, J. Tsukamuto, T. Ishiguro, A.J. Epstein, Synth. Met. 65 (1994) 131.
[44] Y.B. Moon, Y. Cao, P. Smith, A.J. Heeger, Polym. Commun. 30 (1989) 196.
[45] (a) Y.Z. Wang, J. Joo, C.-H. Hsu, J.P. Pouget, A.J. Epstein, Phys. Rev. B 50 (1994) 16811;
(b) Y.Z. Wang, J. Joo, C.-H. Hsu, J.P. Pouget, A.J. Epstein, Synth. Met. 68 (1995) 207.